**Compression Molding and Novel Sintering Treatments for Alnico Type-8 Permanent Magnets in Near-Final Shape with Preferred Orientation**

Aaron G. Kassen[1, 2], Emma M.H. White[1], Wei Tang[1], Liangfa Hu[1], Andriy Palasyuk[1], Lin Zhou[1], Iver E. Anderson[1, 2]

1. Ames Laboratory of the U.S. Department of Energy, Iowa State University, Ames, IA 50011-3020, USA
2. Department of Materials Science and Engineering, Iowa State University, Ames, IA 50011-2300, USA

Contact Author: Iver E. Anderson: andersoni@ameslab.gov

## Abstract

Economic uncertainty in the rare earth (RE) permanent magnet marketplace, as well as an expanding electric drive vehicle market that favors permanent magnet alternating current (AC) synchronous drive motors motivated renewed research in RE-free permanent magnets like "alnico," an Al-Ni-Co-Fe alloy. Thus, high-pressure gas atomized isotropic type-8H pre-alloyed alnico powder was compression molded with a *clean burn-out* binder to near-final shape and sintered to density >99% of cast alnico 8 (full density of 7.3g/cm$^3$). To produce aligned sintered alnico magnets for improved energy product and magnetic remanence, uniaxial stress was attempted to promote controlled grain growth, avoiding directional solidification that provides alignment in alnico 9. Successful development of solid-state powder processing may enable anisotropically aligned alnico magnets with enhanced energy density to be mass-produced.

## Introduction

With the onset of rapid rare earth (RE) price inflation in 2011, traction drive motor manufacturers demanded alternatives to neodymium-iron-boron (Nd-Fe-B) and samarium-cobalt (Sm-Co) type high-energy permanent magnets (HEPM), especially for Nd-Fe-B magnets containing Dy. Alnico was an industry leading HEPM alloy up into the 1970's, prior to the discovery of RE magnets of Sm-Co and Nd-Fe-B with extremely high magnetic energy products (up to ~55 Mega-Gauss·Oersteds (MGOe) for $Nd_2Fe_{14}B$ at room temperature) [1]. Interestingly, the Nd-Fe-B magnets used for drive motors have a typical energy product of ~20 MGOe at 180˚C, the upper operating temperature limit for drive motors. With this more modest energy product objective, RE-free alnico magnets have once again become a candidate for further development in motor applications. Alnico is known for its high magnetic saturation (12-14 kG) and high Curie temperature (about 860˚C), resulting in operation temperatures up to ~500°C, and low coefficients (-0.025%/°C and + 0.01%/˚C) for magnetic inductance and intrinsic coercivity with rising temperature, respectively (for alnico 8, 8H, and 9), unlike Nd-Fe-B magnets with poorer temperature coefficients of -0.11%/°C and -0.60%/°C respectively. To adapt Nd-Fe-B magnets to their current widespread use in drive motors that operate at high temperatures (150-180˚C), Nd is alloyed with Dy, a very costly and uncommon RE metal, and Fe is alloyed with Co.[2] While Sm-Co, the less widely used RE HEPM technology, has insufficient coercivity at operational temperatures for operation in this range without compromise, it also tends to be

unsuitable for motors due to its poor mechanical properties, even compared to Nd-Fe-B. Thus, Nd-Dy-Fe-Co-B magnets, with recent improvements that cut Dy use through grain boundary diffusion processes such as seen at ShinEtsu are currently used as HEPMs for compact traction drives and are the current target for replacement by enhanced RE-free alnico magnets. [2]

Drawbacks of alnico magnets for HEPMs in AC synchronous drive motors has been their low coercivity and energy product [3-5], only ~10 MGOe for fully aligned, anisotropic type-9 magnets, although some alnico magnets have achieved 13 MGOe [6]. However, theoretical calculations have shown that alnico can approach energy products of 30-35 MGOe and coercivities of 4-6 kOe [6-7]. This enhanced alnico would likely consist of a very fine scale **nanostructure** with 10-20nm dia. Fe-Co columns (from spinodal decomposition in an external magnetic field), instead of the typical 30-40nm spinodal, residing within a highly grain oriented **microstructure** which aligns the magnetic easy axis with that intended for the motor design and should be achievable. Even if more modest energy products are reached for alnico, e.g., 20 MGOe, this would match typical Nd-Dy-Fe-Co-B magnets in today's AC synchronous motors, allowing direct market competition.

Many commercial alnico types have a grain-aligned microstructure resulting from directional solidification and have an anisotropic nano-structure derived from spinodal decomposition in an external magnetic field [7], producing the highest energy products in types 5, 5-7, and 9 [8]. Fortunately, materials processing and characterization advances present opportunities for dramatically enhanced alnico magnets, allowing preconceived notions about alnico alloys and processing to be challenged [7]. For example, alnico 8 is currently understood to derive its good intrinsic coercivity (compared to alnico 9) primarily from shape anisotropy, resulting from elongation of the nanostructured Fe-Co spinodal rods. However, if the reduced remnant magnetization of type-8 with its isotropic microstructure [5] could be increased by a solid state method, the microstructure could be aligned without reducing its coercivity greatly increasing the energy product.

Encouragement for this pathway comes from early single crystal and texturing experiments performed by Durrand-Charre and Liu who showed, when preferred microstructural orientation is promoted, improved magnetic energy product and remanent magnetization are possible [9-10]. Specifically, Durrand-Charre showed, if preferential orientation could be achieved in alnico

within approximately 15 degrees of the optimal [100] alignment, enhanced properties could be achieved over typical isotropic magnets, in agreement with Chikazumi and Bunge [10-13].

## Experimental

Using high-pressure gas atomization (HPGA) at Ames Laboratory, an alnico 8H pre-alloyed powder was produced and size classified as previously detailed in Anderson et al. [14-15]. Elemental charge additions were of commercial high purity (99.99%) with some pre-melted into master alloy buttons. The charge was homogenized and superheated to 1625°C and atomized by high purity argon gas supplied at 2.93 MPa (425 psi).

A powder sample in the form of 90wt.% 32-38μm + 10wt.% 3-15μm was compounded with a 6wt.% solution of a polypropylene carbonate binder (QPAC 40®), noted for its clean burnout characteristics [14]. Samples of the blended material were compression molded into two different cylindrical dies: 0.9525cm (dia.) at 156 MPa and 2.54cm (dia.) at 175 MPa, to create "green bodies" suitable for de-binding and sintering processes. Binder burnout was detailed in Anderson et al. and vacuum sintering experiments were performed between 1-12h at 1250°C, below the solidus of 1281°C, from differential scanning calorimetry, to produce samples with density >99% (cast density = 7.3 g/cm$^3$) [15,17]. Experimental specimens were cut from bulk specimens to 3.25mm (dia.) and centerless ground to 3mm and 8mm length with parallel ends.

Two different processing paths were compared for sintered specimens. Non-stressed control groups of specimens were vacuum sintered for 1 to 12h to measure densification rate and magnetic properties. A second series of specimens received a primary (4h) sintering step to 99% dense, followed by a novel grain growth step under an applied uni-axial stress during secondary sintering for 4h. Stressed specimens were placed in a uniaxial loading apparatus (Fig. 1) for the secondary 4h sintering treatment in vacuum (<5 x $10^{-6}$torr) at 1250˚C. Applied stress varied up to 1,248 kPa (900g) to determine the effect of the stress on the development of microstructure. The highest pressures were excursion limited to approximately 10% axial strain, which resulted in a reduction of applied stress at the limit, while lower pressures, less than 345 kPa (250g), allowed continuous strain to occur during the experiment at a continuous pressure. After the stress-biased grain growth process was completed, centerless grinding was performed a second time. All finished samples received a final solutionizing (1250°C, 30 minutes) heat treatment and oil

quench, followed by magnetic annealing (1.0T, 840°C, 10 minutes) and draw annealing cycles at 650°C for 5h and 580°C for 15h. Magnetic properties were measured with a closed loop Laboratorio Elettrofisico AMH-500 hysteresisgraph at a maximum applied field of 12 kOe [14].

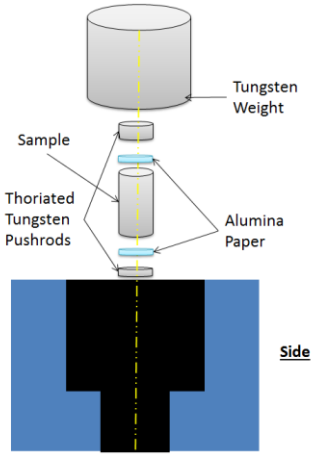


*Figure 1 Schematic of uni-axial loading apparatus for alnico specimen texturing.*

SEM analysis of longitudinal microstructures and grain orientation were performed using an Amray 1845 scanning electron microscope (SEM), JEOL JAMP-7830F Auger electron spectroscopy system, and a FEI Teneo SEM, each fitted with an electron backscatter detector (EBSD) to determine final grain size and to obtain orientation-mapping data to correlate with magnetic properties.

## Results and Discussion

### *Compression Molding & Sintering:*

Chemical analysis of the as-atomized (dia.<45µm) powder (NSL Analytical, Cleveland, OH) verified that the match between the desired and final compositions was nearly perfect. Inert gas fusion analysis of dia.<45µm powder revealed bulk oxygen of 190 ppmw, less than half of aerospace specifications. Carbon determination showed a maximum of 209 ppmw (8h sintered sample), below industry values of 300 ppmw [17], verifying that binder decomposition produced no significant carbon increase in the final sintered magnets.

Compression molding formed near-final shape magnets as detailed in Anderson et al., producing green bodies with geometric measured average relative densities of 70% of cast density [15,16]. After de-binding and final sintering, shrinkage was consistently predictable, with approximately 10% lineal shrinkage occurring for samples sintered for 8h and about 9% shrinkage for samples sintered for 4h. Final sintering and debinding curves were established experimentally and a densification curve was established, showing rapid densification in the first 0.5h and about 99% density by 4h.

Residual porosity in the micrographs of Fig. 2 agreed with measured Archimedes density values. The sample in Fig. 2c initially appeared to show higher than expected porosity along prior particle boundaries. However, further examination and EDS mapping confirmed that the micro-scale features were spheroidized alumina particles that developed during sintering from the original passivating oxide layer present on the atomized powder.

Grain contrast imaging in backscattered SEM analysis permitted grain size to be measured in each specimen, indicating average grain sizes of 23µm, 30µm, and 1.3mm, after sintering for 1h, 4h, and 8h, respectively. Interestingly, most spheroidized alumina particles that were observed (Fig. 2c) decorating prior particle boundaries from the initial HPGA powder became intragranular, showing that they were not effective at pinning the grain boundaries after extended sintering at 1250˚C.

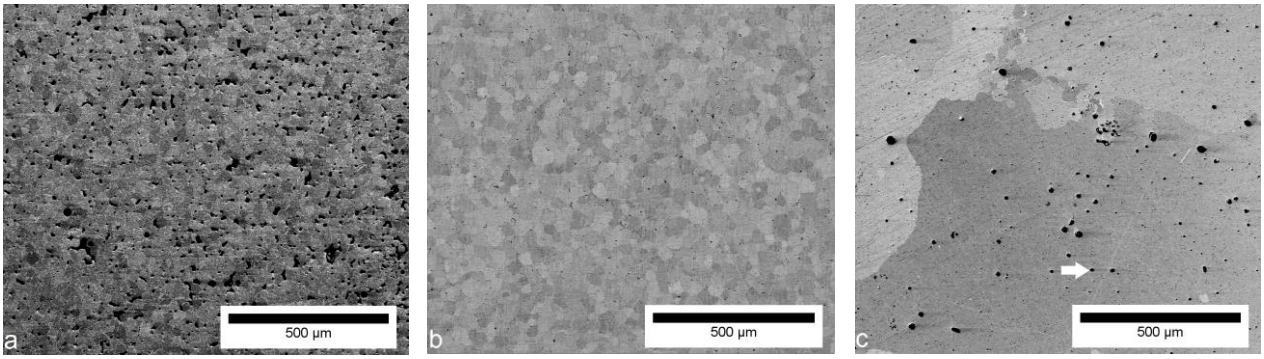


*Figure 2. SEM (BSE) images of 1250°C sintered samples: a) 1h; Archimedes 98.8% dense, b) 4h sinter; 99.1% dense, and c) 8h sinter; 99.6% dense sintered samples showing grain contrast and residual porosity. Also observed in the 8h sinter micrograph is coarsened spheroidized alumina particles decorating prior particle boundaries, e.g., indicated by the arrow in (c) verified by EDS mapping.*

***Uniaxial Stress Application during Extended Sintering:***

A uniaxial compressive stress was applied to samples in the as-sintered 4h condition. The fixture ensured a uniaxial stress condition in each 3mm (dia.) x 8mm (height) specimen, ranging up to 1,248 kPa (900g) applied along the longitudinal axis of the cylindrical specimens. The secondary sintering temperature of 1250°C and a time of 4h were used with the uniaxial stress application since it was known to promote abnormal grain growth in the occasional sample, as discussed earlier and detailed in Anderson et al. [14].

Any resulting plastic deformation or shear/creep that was promoted by each level of stress was measured as the growth of the diameter and shrinkage of the height of each specimen measured at the bottom, middle, and top of respective samples. Resulting plastic deformation of the post-treatment specimens, as a function of stress level, are shown in Figure 3. This plot extends only up to samples stressed to 345 kPa (250g) to illustrate the results of the most reliable experiments. Some samples that were subjected to 1,248 kPa (900g) had height decrease and diameter expansion values that were "excursion limited" by the fixture dimensions, where the post-test plastic strain averaged approximately +8% in the diameter and -11% in height.

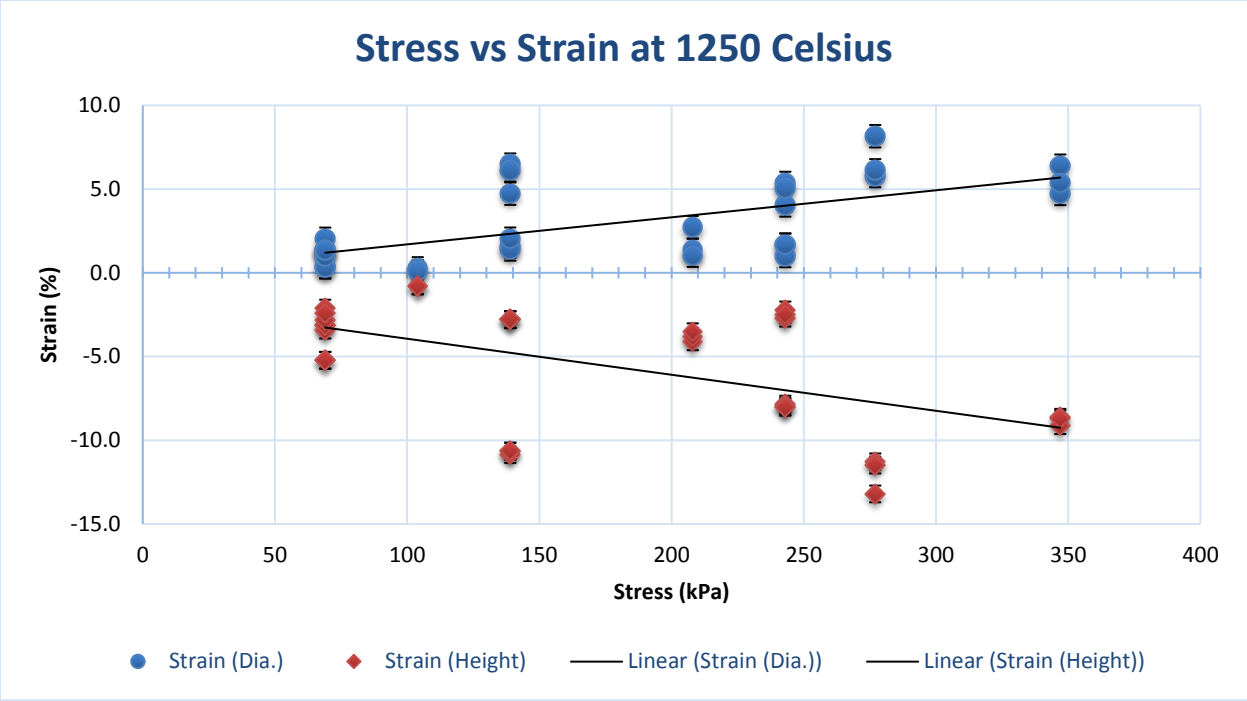


*Figure 3. Summary of results for applied stress vs. strain plot for alnico held 4h at 1250°C.*

In longitudinal sections of the resultant microstructures, EBSD showed that after plastic deformation at 1250°C, samples subject to the highest loads of 1,248 kPa were observed to have a primarily <111> final texture in the normal direction and near <110> type texture along the axial direction (see Fig. 4a). This is consistent with slip systems under uniaxial compression activated in the body-centered cubic (BCC) structure, where the compressive axis should align itself with the normal to the slip plane and, the slip direction normal will rotate away from the compressive axis [18]. This would be indicative of classic BCC pencil-glide and grain rotation at these elevated temperatures, which determines the texture that evolved during the apparent shear/creep and grain growth within the samples [18].

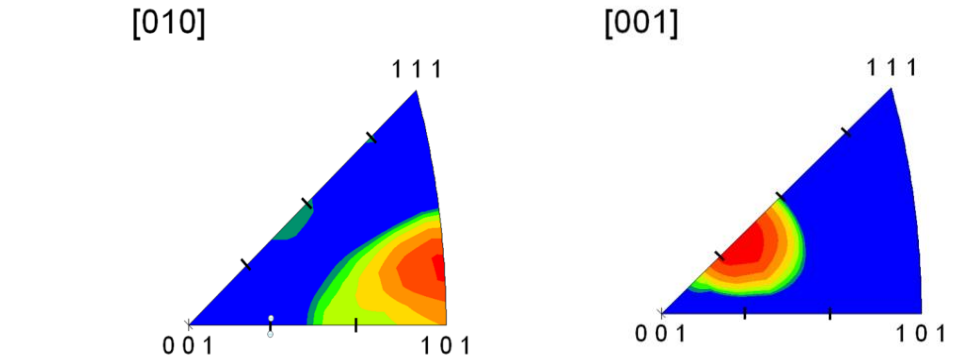


a) b)

*Figure 4. Representative orientation summaries showing two distinct identified modes: a) inverse pole figure along the axial direction for 900g loading (with 15-degree tick marks), and b) inverse pole figure along the axial direction for 75g loading (with 15-degree tick marks).*

Final orientation of the normal to the slip planes from the grain rotation mechanism (Fig. 4a) means the orientation of any easy magnetization direction with respect to the axial direction is clearly sub-optimal. Optimal orientation would be an alignment of the <001> easy direction with magnet sample axial direction in this case. Reduction in magnetic properties for misoriented microstructures from ideal alignment can be approximated with a Schmidt style law approach that involves two rotations (theta-phi) to align the crystal and axial coordinate systems to any <001> type direction [19]. However, a simple approximation can be derived by considering a simple tilt angle of approximately 45˚ between the axial direction and plane normal resulting from the alignment and the desired <001> orientation. In this situation (~45˚ misalignment), we are approaching a minimum for magnetic properties for cubic symmetry as indicated in works by both Higuchi and Zhou that shows the angular relationship between crystal orientation and magnetic properties of alnico [19-20]. The resulting magnetic properties for Fig. 4a corresponded to a reduction in all texture related parameters (i.e. magnetic remanence, energy product, and remanence ratio) with $B_r$ of 8.41 kG, remanence ratio of only 0.71, and reduced energy product of 4.34 MGOe. This shows a reduction in magnetic properties over the starting condition isotropic magnets which typically would have a $B_r$ of 8.8 kG, remanence ratio of 0.72 and energy product on the order of 5 MGOe.

In contrast, samples stressed below about 250g resulted in a distinct improvement in texturing characteristics (Fig. 4b) as compared to the high stress/strain situation (Fig. 4a). The sample for Fig. 4b showed enhanced texture corresponding to its near [001] orientation with improvements in all texture related properties with $B_r$ of 9.01 kG, remanence ratio of 0.76, and an energy product of 5.02 MGOe. The measured tendency to align near the <115> direction (see Fig. 4b) resulted in an orientation close to the ideal orientation of [001]. The application of a sufficient low uni-axial stress seems to induce a slightly anisotropic grain boundary energy that prefers anisotropic grain boundary mobility; producing grain growth bias in this cubic system with nearly isotropic grain boundary energy. Subsequent experiments have been able to enhance these parameters even further to a remanence ratio of 0.79 and energy product of 5.65 MGOe.

Therefore, two distinct textures can be achieved depending on the mechanism employed, either grain rotation and growth that would require post-process shaping/machining to utilize its preferred orientation advantage or grain boundary energy biased growth that could be used directly as a near-final shape magnet. The latter case with low-stress levels may be more suitable to simplified mass production methods. The fully optimized texture should result in further increase of remanence ratio values, creating an improved energy product and square hysteresis loop shape that is desired by motor manufacturers.

## Conclusions

Gas atomized pre-alloyed alnico powder was used to create a highly dense fine-grained sintered alnico microstructure that is a starting condition for controlled abnormal grain growth processing that can convert weak isotropic magnets into HEPM alnico magnets with a large-grained aligned microstructure. This novel process, which could be utilized in different powder metallurgical systems that also undergo the AGG process, employs uni-axial stressing of sintered alnico with a static load in a solutionized (BCC) phase field at very high temperatures (>0.97 $T_{solidus}$). Two rapid grain growth mechanisms can be promoted to create different microstructural textures: either plastic deformation induced grain rotation at high loads or, preferably, grain boundary energy biased grain growth at low loads. Using this solid-state approach at low loads, an alnico alloy that has a large-grained, distinctly textured microstructure, approaching the 15-degree beneficial threshold of Durand-Charre, was demonstrated with an improvement of 30% in energy product over the highly stressed grain rotation case.

**Acknowledgements**

The authors wish to acknowledge the invaluable assistance rendered by David Byrd, Ross Anderson, Rick Schmidt, and Steve Constantinides. This work was supported by DOE-EERE-VT-EDT (Electric Drive Technologies) Program at the Ames Laboratory, operated for the U.S. DOE by Iowa State University under contract no. DE-AC02-07CH11358.

## References


1. R. A. McCurrie, *Ferromagnetic Materials: A Handbook on the Properties of Magnetically Ordered Substances*, ed. E.P. Wohlfarth (North-Holland Physics Publishing: 1982), pp 107-188.
2. S. Sugimoto, *J. Phys. D: Appl. Phys.* (2011) doi:10.1088/0022-3727/44/6/064001.
3. Chad D Graham and Bernard D. Cullity, *Introduction to Magnetic Materials*. 2nd ed. (John Wiley & Sons, Hoboken, 2009), pp. 485-487.
4. Emma M. White, Aaron G. Kassen, Kevin W. Dennis, Andriy Palasyuk, R. William McCallum, and Iver E. Anderson, Int. J. Powder Metall., 52, 33-39 (2016).
5. Lin Zhou, M. K. Miller, Ping Lu, Liqin Ke, R. Skomski, H. Dillon, Q. Xing, A. Palasyuk, M. R. McCartney, D. J. Smith, S. Constantinides, R. W. McCallum, I. E. Anderson, V. Antropov and M. J. Kramer, *Acta Mater.* , 74, 224 (2014).
6. K. J. De Vos, *Magnetism and Metallurgy*, ed. Ami E. Berkowitz and Kneller Eckart (Academic Press INC: New York, 1969), pp 473-511.
7. Pieter A. Naastepad, *Z. Angew. Phys. ,* 21, 104 (1966).
8. M. J. Kramer, R. W. McCallum, I. A. Anderson and S. Constantinides, *JOM* , 64, 752 (2012).
9. Arnold Magnetic Technologies, "Alnico Magnets" (Arnold Magnetics Technolgies,2015), http://www.arnoldmagnetics.com/en-us/Products/Alnico-Magnets. Accessed 03/13/2017.
10. Claude Bronner, Madeline Durand-Charre, and Jean-Pierre Lagarde, *IEEE Trans. Magn.* , Mag-14, 797 (1978).
11. Tao Liu, Wei Li, Minggang Zhu, Zhaohui Guo and Yanfeng Li, *J. Appl. Phys.* (2014) doi: 10.1063/1.4868083.
12. Sōshin Chikazumi, *Physics of ferromagnetism; English edition prepared with the assistance of C.D. Graham, Jr.*, 2 ed. (Oxford University Press, Oxford University Press Inc. United States, 1999), pp 27-31.
13. H. J. Bunge, *Textures and Microstruct.* , 11, 75 (1989).
14. I. E. Anderson, A. G. Kassen, E. M. H. White, L. Zhou, W. Tang, A. Palasyuk, K. W. Dennis, R. W. McCallum and M. J. Kramer, *J. Appl. Phys.* (2015) doi: 10.1063/1.4916996.
15. I. E. Anderson, D. Byrd and J. Meyer, *Materialwiss. Werkstofftech.* , 41, 504 (2014).
16. *American Society for Metals, In Metals Handbook: Desktop Edition, ed. Howard E. Boyer and Timothy L Gall (American Society for Metals: Metals Park, OH, 1985) pp. 20•10-11.*
17. Steve Constantinides, Arnold Magnetics Technologies, Rochester, NY, Unpublished Private Communication, 2014.
18. William F. Hosford, *Mechanical Behavior of Materials,* (Cambridge University Press, 2009), pp. 120-125.
19. A. Higuchi, T. Miyamoto, *IEEE Trans.Magn.*, MAG-6, 218 (1970).
20. Lin Zhou, M. K. Miller, H. Dillon, A. Palasyuk, S. Constantinides, R. W. McCallum, I. E. Anderson and M. J. Kramer, *Metall. Mat. Trans. E* , 1, 27 (2014).